First International Symposium on Marine Propulsors
smp'09, Trondheim, Norway, June 2009

Propulsion Control Strategies for Fixed Pitch Propellers at Low Advance Speed

Asgeir J. Sørensen[1], Øyvind Smogeli[2] and Eivind Ruth[3]

[1]Department of Marine Technology, NTNU, Trondheim, Norway
[2]Marine Cybernetics, Tiller, Norway
[3]Det Norske Veritas, Høvik, Norway

ABSTRACT

Positioning control systems for marine vessels include different control functions for station-keeping, maneuvering, and transit operations by means of proper action of the propulsion system. This paper presents an overview of the various propulsion control strategies for fixed pitch propeller (FPP) at low advance number based on thruster shaft speed, torque, and power control. It can be shown that significant reduction in power and torque fluctuations can be achieved in waves. In high seas, however, when the propeller may be subject to large thrust losses due to ventilation and in-and-out-of-water effects, torque and power thruster control will lead to propeller racing. To facilitate use of torque and power control also in high seas, an anti-spin thruster controller is proposed.

1 INTRODUCTION

Electrical propulsion has during the last decade become the preferred solution for offshore vessels, cruise and passenger ships. This opens up for new control solutions combining the disciplines of hydrodynamics, electrical power, and control engineering. The real-time control hierarchy of a marine control system may be divided into three levels: the *guidance system*, the *high-level plant control* (e.g. dynamic positioning controller including thrust allocation), and the *low-level thruster control* (Sørensen, 2005). In this paper an overview of modelling and control of electrically driven FPP on vessels at low advance speed is given. The paper summarize some of the main results from Sørensen and Smogeli (2009), Smogeli and Sørensen (2009), Smogeli (2006) and Ruth (2008). Related research can be found in the following references: Blanke and Busk Nielsen (1987), Blanke and Busk Nielsen (1990), Blanke (1994), Sørensen et al. (1997), Smogeli et al. (2003, 2004b,a, 2005, 2008), Ruth et al. (2006), Pivano (2008), Bakkeheim et al. (2008), and Blanke et al. (2007). Various governor control schemes for diesel engines with direct mechanically driven propellers are presented in Blanke and Busk Nielsen (1990), and are not further treated here. Unless otherwise stated, it will in this paper be referred to tunnel thrusters, azimuthing thrusters, pods, and main propellers as thrusters or propellers.

In the current work, two operational regimes are defined: normal and extreme conditions. In normal operating conditions, i.e. calm to moderate seas, the dynamic loading of the propeller due to thrust and torque losses is considered to be moderate. In extreme operating conditions, i.e. high to extreme seas, the thrusters may be subject to ventilation and in-and-out-of water effects. This leads to large transients in propeller loading, and hence in thrust and power, see e.g. Faltinsen et al. (1980), Minsaas et al. (1987), Koushan (2004), Smogeli et al. (2004a), Ruth and Smogeli (2006), and the references therein. For vessels with diesel-electric propulsion systems, the thrusters are normally the main power consumers. The thruster control system performance is therefore critical for avoiding blackouts and harmonic distortions in the power generation and distribution system. In extreme conditions, the control systems designed for normal operating conditions may be inadequate, and lead to increased mechanical wear and tear and unpredictable power consumption. Motivated by the similar problem of a car wheel losing friction on a slippery surface during braking or acceleration, the concept of anti-spin thruster control was introduced in Smogeli et al. (2003, 2004a), Smogeli (2006), and Smogeli et al. (2008). In Ruth (2008) anti-spin thruster allocation is treated. Ruth shows in his work how thrust may be re-allocated to non-ventilating propellers, increasing overall efficiency and improving thrust production. Thrust allocation will not be considered in this paper.

2 PROPELLER MODELLING

This section treats modelling of propellers from a control point of view. This means that the models are required to be accurate enough to capture the main physical effects, and such facilitate control system design and testing. The actual propeller thrust T_a and torque Q_a are influenced by many parameters, the most important being propeller geometry, submergence, and propeller loading – which depends on the propeller pitch ratio and shaft speed. T_a and Q_a can in

general be formulated as functions of fixed thruster parameters θ_p (i.e. propeller diameter, geometry, position, etc.), the shaft speed n, and variables $\mathbf{x}_p$ (i.e. pitch ratio, advance velocity, submergence, etc.):

$$T_a = f_T(n, \mathbf{x}_p, \theta_p), \tag{1a}$$
$$Q_a = f_Q(n, \mathbf{x}_p, \theta_p). \tag{1b}$$

In the following, only speed controlled FPP will be considered. The pitch ratio will in this case be a fixed parameter. Further, only thrusters and propellers with low advance number on dynamically positioned (DP) vessels are considered. DP includes station-keeping and low-speed tracking, and implies that the thrusters are subject to small water inflow velocities. The models are, however, easily extendable to both controllable pitch propellers (CPP) and higher inflow velocities, as experienced on vessels in transit, see Smogeli (2006), Ruth et al. (2006) and Ruth (2008). The functions $f_Q(\cdot)$ and $f_T(\cdot)$ may include loss effects due to e.g. in-line and transverse velocity fluctuations, ventilation, in-and-out-of water effects, and thruster-thruster interaction, as well as dynamic flow effects.

2.1 Motor and Shaft Dynamics

The electric motor torque Q_m is controlled by a high bandwidth inner torque control loop. The resulting motor torque dynamics is in this work considered to be negligible when compared to the rotational dynamics of the propeller shaft. Hence, the motor torque Q_m may be replaced by the commanded torque Q_c from the thruster controller. The rotational dynamics of the propeller and shaft is then defined in terms of the moment of inertia for shafts, gears and propeller I_s, the angular velocity $\omega = 2\pi n$, the commanded torque Q_c, the propeller load torque Q_a, and the shaft friction $Q_f(\omega)$ according to:

$$I_s\dot{\omega} = Q_c - Q_a - Q_f(\omega). \tag{2}$$

$Q_f(\omega)$ may for most applications be viewed as a sum of a static friction (or starting torque) $Q_s \geq 0$ and a linear component $K_\omega\omega$, where $K_\omega \geq 0$ is a linear friction coefficient. Consequently:

$$Q_f(\omega) = \tanh(\omega/\varepsilon)Q_s + K_\omega\omega, \tag{3}$$

where $\varepsilon > 0$ is an appropriately chosen small constant.
More sophisticated models of the shaft dynamics, where also flow dynamics are included, have been developed and analyzed by Yoerger et al. (1991), Healey et al. (1995), Whitcomb and Yoerger (1999a), Bachmayer et al. (2000), and Fossen and Blanke (2000). Such models have not been considered for the current work, since they were developed for deeply submerged propellers, and cannot account for the large thrust losses that occur when the propeller is subject to ventilation and in-and-out-of water effects.

2.2 Propeller Characteristics

The relationships between the actual propeller thrust T_a, torque Q_a, shaft speed n, diameter D, and density of water ρ are commonly given in the form of the thrust and torque coefficients $K_T(n, \mathbf{x}_p, \theta_p) \geq 0$ and $K_Q(n, \mathbf{x}_p, \theta_p) \geq 0$ according to:

$$T_a = f_T(\cdot) = \text{sign}(n)K_T(n, \mathbf{x}_p, \theta_p)\rho D^4 n^2, \tag{4}$$
$$Q_a = f_Q(\cdot) = \text{sign}(n)K_Q(n, \mathbf{x}_p, \theta_p)\rho D^5 n^2. \tag{5}$$

The strictly positive propeller power consumption P_a may be written as:

$$P_a = 2\pi n Q_a = \text{sign}(n)2\pi K_Q(n, \mathbf{x}_p, \theta_p)\rho D^5 n^3. \tag{6}$$

For a given propeller geometry, K_T and K_Q will for notational simplicity be written as functions of the angular velocity ω and time t, with time representing the exogenous thrust losses: $K_T(\cdot) = K_T(t, \omega)$, and $K_Q(\cdot) = K_Q(t, \omega)$. The nominal thrust T_n, torque Q_n, and power P_n for a deeply submerged propeller with no thrust losses are given by the constant nominal thrust and torque coefficients for zero advance number $V_a = 0$, $K_{T0} > 0$ and $K_{Q0} > 0$:

$$T_n = \text{sign}(n)K_{T0}\rho D^4 n^2, \tag{7a}$$
$$Q_n = \text{sign}(n)K_{Q0}\rho D^5 n^2, \tag{7b}$$
$$P_n = 2\pi n Q_n = \text{sign}(n)2\pi K_{Q0}\rho D^5 n^3. \tag{7c}$$

When a propeller is subject to waves, current, and vessel motion, it will experience a time-varying water inflow (advance velocity). This leads to oscillations in the shaft speed, thrust, torque, and power about their nominal values given by (7a)-(7c), depending on the thruster control scheme.

2.3 Thrust Loss Effects

Modelling of thrust losses is most commonly solved by empirical methods in conjunction with analytical models. The following loss effects may be considered:

- Fluctuations in the in-line water inflow to the propeller will cause fluctuations in thrust and torque.
- Water inflow perpendicular to the propeller axis will introduce a force in the direction of the inflow due to deflection of the propeller race, termed transverse losses. This is often referred to as cross-coupling drag for open and ducted propellers (Lehn, 1992), and speed or suction loss for tunnel thrusters, see Chislett and Björheden (1966) or Brix (1978).
- For heavily loaded propellers ventilation (air suction) caused by decreasing pressure on the propeller blades may occur, especially when the effective submergence of the propeller becomes small due to waves and wave-frequency motions of the ship, see e.g. Shiba

(1953). If the relative propeller motion results in water exits, additional losses due to in-and-out-of-water effects following a hysteresis pattern similar to the Wagner effect will occur, see e.g. Faltinsen et al. (1980) or Smogeli (2006) and the references therein. These losses mostly affect tunnel thrusters and main propellers.

- For azimuthing thrusters, both thrust reduction and change of thrust direction may occur due to thruster-hull interaction caused by frictional losses and pressure effects when the thruster race sweeps along the hull (Lehn, 1992). The last is referred to as the Coanda effect.

- Thruster-thruster interaction caused by influence from the propeller race from one thruster on neighboring thrusters may lead to significant thrust reduction, if not appropriate precautions are taken in the thrust allocation algorithm, see e.g. Lehn (1992) or Koushan (2004).

The sensitivity to the different types of losses depends on the type of propeller and thruster used, application of skegs and fins, hull design and operational philosophy. The effect of the above mentioned thrust losses may be expressed by the thrust and torque reduction coefficients β_T and β_Q, which express the ratio of the actual to the nominal thrust and torque (Minsaas et al., 1987):

$$\beta_T(t,\omega) = T_a/T_n = K_T(t,\omega)/K_{T0}, \quad (8)$$

$$\beta_Q(t,\omega) = Q_a/Q_n = K_Q(t,\omega)/K_{Q0}. \quad (9)$$

In order to improve the understanding of thrust losses due to ventilation and in-and-out-of-water effects, systematic experiments in the cavitation tunnel at NTNU have recently been performed. As an example, Figure 1 shows the relative thrust $T/T_{\max}$ as a function of the relative submergence h/R and the shaft speed n for a ducted propeller. h is the propeller shaft submergence, R is the propeller radius, T is the measured thrust, and $T_{\max}$ is the maximum thrust observed in the experiments. For large h/R, the thruster performs as expected, with thrust proportional to n^2. For low shaft speeds, and hence low propeller loading, the thrust is constant for $h/R = 1.5$ to $h/R = 1$, and then decays almost linearly from $h/R = 1$ to $h/R = 0$. This corresponds to lost thrust due to loss of effective disc area (Minsaas et al., 1987). If the propeller loading is sufficiently high, the low pressure on the propeller blades may create a funnel through which air is drawn from the free surface, thus ventilating the propeller (Shiba, 1953). For a heavily loaded propeller, ventilation may lead to an abrupt loss of thrust and torque as high as 70-80%. Figure 1 indicates that a reduction of shaft speed in such a case may increase the thrust, and that an increase in shaft speed will not increase the thrust. In the following, "ventilation losses" and "ventilation incidents" will be used as common terms for the above mentioned loss effects. A simplified simulation model based on the experimental results is presented in Smogeli et al. (2008) and Smogeli (2006).

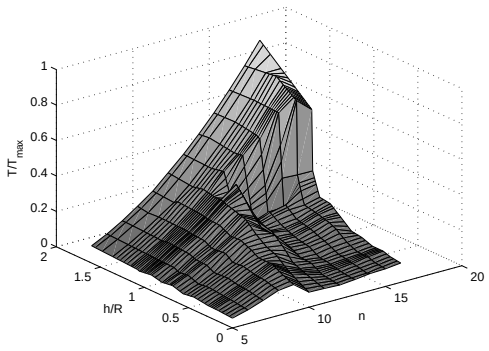

Figure 1: Relative thrust $T/T_{\max}$ as a function of relative submergence h/R and propeller shaft speed n, from experiments.

The mechanical effects of the dynamic loading of the propeller during ventilation, typically at shaft frequency, blade frequency, and above, is also an important topic. There are few available references considering such dynamic loads, but a summary of previous findings and a thorough investigation of dynamic load effects can be found in Olofsson (1996). Although not well documented in literature, industrial experience shows that the high thrust losses combined with wave-frequency cyclic variations in propeller loading may lead to severe mechanical wear and tear of the propulsion unit (Koushan, 2004). According to Olofsson (1996), the dynamic loads during ventilation increase with the propeller shaft speed. It is, therefore, considered beneficial to avoid high shaft speeds during ventilation.

3 LOW-LEVEL THRUSTER CONTROLLERS

The purpose of the low-level thruster controller is to relate the desired thrust T_d, given by the thrust allocation routine, to the commanded motor torque Q_c. The thruster controllers may be divided in two control regimes, depending on the operational conditions:

(a) Thruster control in normal conditions, when experiencing low to moderate thrust losses.

(b) Thruster control in extreme conditions, when experiencing large and abrupt thrust losses due to ventilation and in-and-out-of-water effects.

For surface vessels with FPP, shaft speed control is the industry standard, whereas torque and power control was introduced by Sørensen et al. (1997), and a combined torque and power controller was presented in Smogeli et al. (2004b). For underwater vehicles, both torque and various shaft speed control schemes have been proposed, see

Yoerger et al. (1991), Whitcomb and Yoerger (1999b), Fossen and Blanke (2000), and the references therein. For control of diesel engines, shaft speed control is the most commonly used solution. However, both torque and power control have been proposed and implemented, see Blanke and Busk Nielsen (1987, 1990).

3.1 Control Objectives

Shaft speed feedback control is the conventional way to control a FPP. However, as will be shown later, this may not be the best design choice. The ultimate goal of any thruster controller is to make the actual thrust track the desired thrust. Since no feedback from the actual thrust is available, different ways of trying to achieve this for a FPP are:

- Shaft speed feedback control.
- Torque feedforward control.
- Power feedback control.
- Combinations of the above.

In dynamic operating conditions, other goals may be more important than tracking the desired thrust, e.g. reducing mechanical wear and tear, and limiting power oscillations and peak values. Predictable power consumption is of major concern to the power management system in order to avoid blackouts and improving the performance and the stability of the electrical power plant network. Other performance criteria than thrust production should therefore also be taken into account. In this work, the following performance criteria are considered:

1. Thrust production in presence of disturbances, i.e. ability to locally counteract thrust losses.
2. Mechanical wear and tear caused by transients and oscillations in motor and propeller torque.
3. Predictable power consumption.

4 THRUSTER CONTROL IN NORMAL CONDITIONS

4.1 Controller Structure

The low-level thruster controller is proposed to be composed of five main building blocks: reference generator, core controller, inertia compensation, friction compensation, and torque limiting. This is shown in Figure 2, where a block diagram of a thruster with low-level thruster controller is presented. The commanded torque from the core controller is termed Q_{ci}, where $i = n$ for shaft speed control, $i = q$ for torque control, $i = p$ for power control, and $i = c$ for combined torque/power control. The commanded torque from the friction and inertia compensation schemes are termed Q_{ff} and Q_{if}, respectively, and the total commanded torque before torque and power limiting Q_{c0} is given by:

$$Q_{c0} = Q_{ci} + Q_{ff} + Q_{if}. \tag{10}$$

Q_{c0} is then limited by a torque and power limiting function to yield the commanded torque to the motor Q_c.

4.2 Control Plant Model Parameters

Since the propeller diameter D and density of water ρ are known and constant, the only remaining parameters are the thrust and torque coefficients K_T and K_Q. The thrust and torque coefficients used in the controllers are termed K_{TC} and K_{QC}, and denoted control coefficients.

4.2.1 Choosing K_{TC} and K_{QC}

In thruster control for station-keeping operations, estimates of the nominal thrust and torque coefficients K_{T0} and K_{Q0} are usually chosen as control coefficients, because the actual advance velocity is unknown to the controller. Doppler logs, GPS, or similar may be used to give estimates of the advance velocity, but these measurements are usually not of sufficient accuracy for inclusion in the low-level thruster controllers.

For thruster control in transit, only the main propellers of the vessel are used. If the propeller characteristics are known, improved controller performance may be achieved by estimating the propeller advance velocity V_a using the known vessel surge speed U and an estimated hull wake factor, or a low-pass filtered measurement from a Doppler log or GPS. K_{TC} and K_{QC} could then be estimated from the propeller characteristics. Similar reasoning may be applied to an underwater vehicle, where the propeller normally is deeply submerged and not subject to wave effects, ventilation and water exits. Such an output feedback shaft speed controller with advance speed compensation for AUVs can be found in Fossen and Blanke (2000). In the following, station-keeping and low-speed manoeuvring operations of surface vessels are of main concern, such that the control coefficients are taken as K_{T0} and K_{Q0}.

4.2.2 Reverse Thrust

With the exception of tunnel thrusters, most propellers are asymmetric. To achieve good performance for both positive and negative thrust references, it may therefore be necessary to use two sets of control parameters. For low-speed operations, this means that K_{T0} and K_{Q0} should be used for positive T_r, and the reverse thrust coefficients K_{T0r} and K_{Q0r} for negative T_r. The following control coefficients are therefore proposed:

$$K_{TC} = K_{T0}\lambda_c + (1 - \lambda_c)K_{T0r}, \tag{11a}$$

$$K_{QC} = K_{Q0}\lambda_c + (1 - \lambda_c)K_{Q0r}, \tag{11b}$$

where λ_c is a smooth switching function given by:

$$\lambda_c = \lambda_c(n_r) = \frac{1}{2} + \frac{1}{2}\tanh(\varepsilon_c \frac{n_r}{n_c}), \tag{12}$$

where $\varepsilon_c > 0$ is a constant. The shaft speed reference n_r is given from T_r by:

$$n_r = g_n(T_r) = \text{sign}(T_r)\sqrt{\frac{|T_r|}{\rho D^4 K_{TC}}}, \tag{13}$$

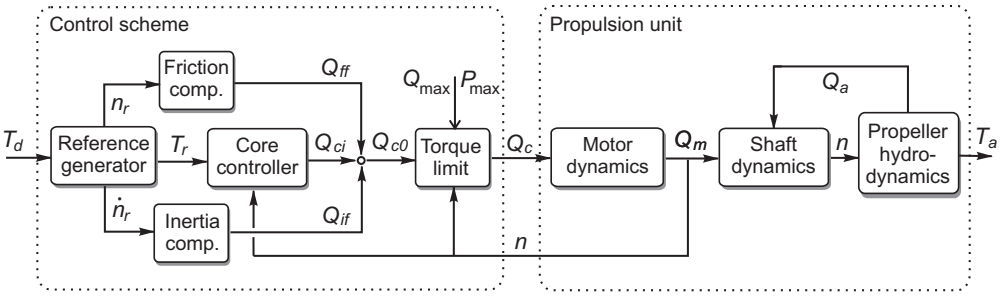

Figure 2: Block diagram of a thruster with reference generator, core controller, inertia and friction compensation, and torque limiting.

which is the inverse function of the nominal shaft speed-to-force characteristics given in (7a) with K_{T0} replaced by K_{TC}. The switch between the coefficients occurs smoothly in the interval $n_r \in [-n_c, n_c]$, such that $\lambda_c \approx 0$ for $n_r < -n_c$ and $\lambda_c \approx 1$ for $n_r > n_c$. The switch "width" n_c may be chosen freely. (11) does not affect the stability properties of the controllers when compared to using constant control coefficients, since K_{T0}, K_{Q0}, K_{T0r}, and K_{Q0r} are strictly positive, and the values of K_{TC} and K_{QC} only affect the mappings from thrust reference to shaft speed, torque, and power reference. Using n_r as the switching variable instead of e.g. the measured shaft speed n means that no measurement noise is entered into the control law through (11).

4.3 Reference Generator

An appropriate reference generator for this system is a second-order filter with rate limiting. The reference generator is imposed on the desired shaft speed n_d, where n_d is given from T_d by g_n in (13), and T_d is given from n_d by the inverse $g_n^{-1}(n_d)$, which is equal to (7a) with K_{T0} replaced by K_{TC}. The second-order filter has damping ratio ζ_r and natural frequency ω_{r0}, and the shaft speed rate limit is set to $\dot{n}_{slew}$, such that the reference generator is given by:

$$\begin{aligned} n_d &= g_n(T_d), \\ \dot{n}_{d2} &= \min(\max(\dot{n}_d, -\dot{n}_{slew}), \dot{n}_{slew}), \\ n_r(s) &= n_{d2}(s)\frac{\omega_{r0}^2}{s^2 + 2\zeta_r\omega_{r0}s + \omega_{r0}^2}, \\ T_r &= g_n^{-1}(n_r). \end{aligned} \tag{14}$$

Notice that the reference generator gives a continuous acceleration reference $\dot{n}_r$, which is available directly from the implementation of the second-order filter.

4.4 Inertia Compensation

For a large thruster, the rotational inertia may be a dominating dynamic term. In order to achieve the desired closed loop properties with respect to response and tracking, it may therefore be beneficial to include an inertia compensation term. The inertial term in the rotational dynamics (2) is $I_s\dot{\omega}$. Since differentiation of the measured shaft speed is undesirable, and the inertia compensation is wanted only when the thrust reference is changed, the following feedforward compensation is proposed:

$$Q_{if}(n_r) = I_c 2\pi\dot{n}_r, \tag{15}$$

where I_c is an estimate of the rotational inertia I_s, and $\dot{n}_r$ is given by the reference generator in (14).

4.5 Friction Compensation

In the torque and power controllers, the friction term $Q_f(\omega)$ will be compensated by a feedforward controller. If this is not the case, and the friction is significant, the controllers will be inaccurate, since at steady state $Q_m \approx Q_a$ no longer holds, see (2). If the shaft friction becomes significant, a feedforward friction term Q_{ff} should therefore be included in the control law. Note that the inclusion of Q_{ff} in the shaft speed controller is unnecessary, since this controller automatically compensates for the friction.
Q_{ff} should be designed to compensate for the friction term $Q_f(\omega)$, i.e. $Q_{ff} \approx Q_f(\omega)$, without destabilizing the system. Therefore a feedforward compensation based on the reference shaft speed n_r from (13) is chosen instead of a destabilizing feedback compensation based on n. Motivated by (3) the friction is assumed to consist of a static and a linear term, and the friction compensation scheme is proposed as:

$$Q_{ff}(n_r) = Q_{ff0}(n_r) + Q_{ff1}(n_r). \tag{16}$$

$Q_{ff0}(n_r)$ is proposed as:

$$Q_{ff0}(n_r) = Q_{f0}\tanh(\varepsilon_f\frac{n_r}{n_s}), \tag{17}$$

where Q_{f0}, $\varepsilon_s > 0$, and n_s are constants. The switch between $-Q_{f0}$ and Q_{f0} occurs smoothly in the interval $n_r \in [-n_s, n_s]$ such that $|n_r| > n_s \Rightarrow Q_{ff0}(n_r) = \text{sign}(n_r)Q_{f0}$, and $n_r = 0 \Rightarrow Q_{ff0}(n_r) = 0$. Note that the switching function is of similar form as the one used in (12). Q_{ff1} is proposed as:

$$Q_{ff1}(n_r) = 2\pi Q_{f1} n_r, \tag{18}$$

where the linear friction coefficient Q_{f1} should be chosen such that $Q_{f1} \approx K_\omega$. In nominal conditions, $n = n_r \Rightarrow Q_{ff1}(n_r) \approx K_\omega \omega$. For $n \neq n_r$, $Q_{ff1}(n_r) \neq K_\omega \omega$, but this only affects the performance about the equilibrium point.

4.6 Torque and Power Limiting

The rated (nominal) torque and power for continuous operation of the motor are denoted Q_N and P_N. The maximum torque and power for the motor are usually set to

$$Q_{\max} = kQ_N, \quad P_{\max} = kP_N, \tag{19}$$

where k typically is in the range of $1.1 - 1.2$. The input to the motor should be limited by a torque limiting function given by:

$$|Q_c| = \min\{|Q_{c0}|, Q_{\max}, P_{\max}/|2\pi n|\},$$

where Q_{c0} is the commanded torque from the controller (10). The maximum power limit yields hyperbolic limit curves for the torque as a function of speed. Since the maximum power is not limited by the converter and motor ratings only, but also by the available power in the generators, this limit should vary accordingly. By this method the power limitation will become fast and accurate, allowing to utilize the power system power capability with a built-in blackout prevention.

4.7 Shaft Speed Feedback Control

For conventional FPP a speed controller is used to achieve the commanded propeller force. Given a specified force command T_r the corresponding reference (commanded) speed of the propeller n_r is found by the shaft speed mapping in (13). The shaft speed PI controller utilizes shaft speed feedback from the thruster, and sets the commanded motor torque Q_{cn} according to

$$Q_{cn} = K_p e + K_i \int_0^t e(\tau) d\tau, \tag{20}$$

where the shaft speed error is $e = n_r - n$, and K_p and K_i are the nonnegative PI gains. The motor torque is controlled by the inner torque control loop, see e.g. Leonhard (1996). K_i is often given as $K_i = K_p/T_i$, where T_i is the integral time constant. The integral term in the PI controller should be limited according to $Q_{\max}$ to avoid integral windup.

4.8 Torque Feedforward Control

In the torque control strategy the outer speed control loop is removed, and the thruster is controlled by its inner torque control loop with a commanded torque Q_{cq} as set-point. A mapping from the reference thrust T_r to the reference torque Q_r can be found from (7a) and (7b) with K_{T0} and K_{Q0} replaced by K_{TC} and K_{QC}. The commanded motor torque Q_{cq} is set equal to the reference torque:

$$Q_{cq} = Q_r = \frac{K_{QC}}{K_{TC}} D T_r. \tag{21}$$

If the response of the thruster is slow, e.g. due to high rotational inertia, the inertia compensation scheme in (15) may be needed to speed up the response. This replaces the "inner torque algorithm" proposed in Sørensen et al. (1997).

4.9 Power Feedback Control

Power control is based on controlling the power consumption of the thruster motor. The inner torque control loop is maintained, and the reference power P_r is found by inserting Q_r from (21) and n_r from (13) in (7c) such that

$$P_r = Q_r 2\pi n_r = |T_r|^{3/2} \frac{2\pi K_{QC}}{\sqrt{\rho} D K_{TC}^{3/2}}. \tag{22}$$

To determine the torque direction, the signed reference power P_{rs} is defined as

$$P_{rs} = \text{sign}(T_r) P_r = \text{sign}(T_r) |T_r|^{3/2} \frac{2\pi K_{QC}}{\sqrt{\rho} D K_{TC}^{3/2}}. \tag{23}$$

The commanded motor torque Q_{cp} is calculated from P_{rs} using feedback from the measured shaft speed $n \neq 0$ according to

$$Q_{cp} = \frac{P_{rs}}{2\pi |n|} = \frac{K_{QC}}{\sqrt{\rho} D K_{TC}^{3/2}} \frac{\text{sign}(T_r) |T_r|^{3/2}}{|n|}. \tag{24}$$

Note that the power controller is singular for zero shaft speed. As in torque control the inertia compensation scheme in (15) may be added if the response of the thruster is slow, replacing the "inner power algorithm" in Sørensen et al. (1997).

4.10 Combined Torque and Power Control

A significant shortcoming of the power control scheme in (24) is the fact that it is singular for zero shaft speed. This means that power control should not be used close to the singular point, for example when commanding low thrust or changing the thrust direction. For low thrust commands, torque control shows better performance in terms of constant thrust production, since the mapping from thrust to torque is more directly related to the propeller loading than the mapping from thrust to power. For high thrust commands, it is essential to avoid power transients, as these lead to higher fuel consumption and possible danger of power blackout and harmonic distortion of the power plant network. Power control is hence a natural choice for high thrust commands. This motivates the construction of a combined torque/power control scheme, utilizing the best properties of both controllers (Smogeli et al., 2004b).

Combining the reference torque from the torque controller Q_{cq} given by (21) and the reference torque from the power controller Q_{cp} given by (24), the commanded motor torque Q_{cc} from the combined torque/power controller is defined as:

$$Q_{cc} = \alpha_c(n) Q_{cq} + (1 - \alpha_c(n)) Q_{cp}. \tag{25}$$

$\alpha_c(n)$ is a weighting function:

$$\alpha_c(n) = e^{-k|pn|^r}, \text{ for } n \in \mathbb{Z}, \tag{26}$$

where k, p and r are positive constants. It satisfies:

$$\lim_{n\to 0} \alpha_c(n) = 1, \quad \lim_{n\to\infty} \alpha_c(n) = 0,$$

and shows smooth behavior for all n. Particularly, $d\alpha_c/dn = 0$ for $n = 0$ and $n \to \pm\infty$. The shape of $\alpha_c(n)$ defines the dominant regimes of the two control schemes, and can be used to tune the controller according to user specifications. The parameter p will act as a scaling factor for n. A small p will widen the weighting function, giving a wider transition between 0 and 1. Increasing the parameter k sharpens the peak about $n = 0$, whereas r widens it and makes the transition from 0 to 1 more steep. The shaft speed is physically limited to some max value $n_{\max}$, such that $\alpha_c(n_{\max})$ should be close to zero. It is easily shown that Q_{cc} is non-singular if $r > 1$. Hence, the power control singularity for $n = 0$ is removed.

The torque and power controllers aim at controlling the motor torque or power, respectively. There is no need for integral action in these controllers, since the motor torque is controlled by its inner torque control loop. Consequently, the torque and power controllers allow the shaft speed of the propeller to vary with the propeller loading, in order to keep the torque or power constant.

5 THRUSTER CONTROL IN EXTREME CONDITIONS

5.1 Loss Estimation and Ventilation Detection

In the development of the anti-spin thruster controller, a scheme for thruster performance monitoring and ventilation detection will be essential. This section presents a load torque observer based on the thruster rotational dynamics in (2), as first presented in Smogeli et al. (2004a) and Smogeli (2006). The load torque estimate can be used to calculate the estimated torque loss factor $\hat{\beta}_Q$. Finally, a ventilation detection scheme based on $\hat{\beta}_Q$ and the measured motor torque Q_m will be developed.

5.1.1 Load Torque Observer

From (2), the following control plant model of the thruster dynamics is proposed:

$$\begin{aligned} I_s\dot{\omega} &= Q_m - Q_a - Q_{ff0}(n_r) - Q_{f1}\omega + \delta_f, \\ \dot{Q}_a &= w_q, \end{aligned} \tag{27}$$

where the measured Q_m has been used instead of Q_c. Since $K_Q(n, \mathbf{x}_p, \theta_p)$ in (5) is unknown and may exhibit highly nonlinear behavior, Q_a is here assumed to be a bias term driven by an exogenous bounded disturbance w_q. This is necessary in order to capture the fast transients during ventilation. The static friction compensation term $Q_{ff0}(n_r)$ from (16) is used instead of a static friction model based on ω in order to avoid oscillations in this term about $\omega \approx 0$. Errors in the friction model are accounted for by δ_f. With the measurement $y = \omega + v$ contaminated with a bounded disturbance v, and $\hat{y} = \hat{\omega}$, a propeller load torque observer copying the control plant model (27) is:

$$\begin{aligned} \dot{\hat{\omega}} &= 1/I_s[Q_m - \hat{Q}_a - Q_{ff0}(n_r) - Q_{f1}\hat{\omega}] + k_a(y - \hat{y}), \\ \dot{\hat{Q}}_a &= k_b(y - \hat{y}), \end{aligned} \tag{28}$$

where k_a and k_b are the observer gains. In Smogeli and Sørensen (2009) it is shown that with a constant load torque Q_a implied by $w_q = 0$, zero measurement disturbance $v = 0$, and perfect friction knowledge such that $\delta_f = 0$, the equilibrium point of the observer estimation error is globally exponentially stable (GES) if the observer gains are chosen as $k_a > -Q_{f1}/I_s$ and $k_b < 0$.

5.1.2 Torque Loss Estimation

For DP operation the expected nominal propeller load torque $\hat{Q}_n$ may be calculated from (7b) by feedback from the propeller shaft speed n. Based on (9), the estimated torque loss factor $\hat{\beta}_Q$ is calculated from $\hat{Q}_a$ in (28) and $\hat{Q}_n$ as:

$$\hat{\beta}_Q = \frac{\hat{Q}_a}{\hat{Q}_n} = \frac{\hat{Q}_a}{K_{QC}\rho D^5 n\,|n|}, \;\; n \neq 0, \tag{29}$$

where the control coefficient K_{QC} (usually equal to K_{Q0}) is used to calculate $\hat{Q}_n$.

Remark 1 *There are no thrust losses for $n = 0$. Hence, the singularity for $n = 0$ is easily avoided by redefining (29) as $\hat{\beta}_Q = \alpha_b(n) + (1 - \alpha_b(n))\hat{Q}_a/\hat{Q}_n$, where $\alpha_b(n)$ is a function of the type (26).*

5.1.3 Ventilation Detection

In this work, the ventilation detection algorithm is implemented by defining limits for the onset and termination of ventilation, $\beta_{v,on}$ and $\beta_{v,off}$, and generating a detection signal by monitoring the thrust loss factor $\hat{\beta}_Q$. An additional criterion for detection is that the magnitude of the motor torque Q_m is non-increasing. A ventilation incident will then give the following evolution of the detection signal ζ, with time instants $t_1 < t_2 < t_3$:

$$\begin{array}{lcl} t_1: & \hat{\beta}_Q > \beta_{v,on} & \Rightarrow \zeta = 0, \\ t_2: & \hat{\beta}_Q \leq \beta_{v,on} \cap \operatorname{sign}(Q_m)\dot{Q}_m \leq 0 & \Rightarrow \zeta = 1, \\ t_3: & \hat{\beta}_Q \geq \beta_{v,off} & \Rightarrow \zeta = 0. \end{array} \tag{30}$$

To avoid switching and chattering of the detection signal due to measurement noise and transients, an algorithm implementing a detection delay is added, such that once ventilation has been detected, it cannot be reset until after a given time interval T_{vent}. The detection delay can be seen as an implementation of the switching dwell-time proposed in Hespanha and Morse (2002). This ventilation detection scheme has shown good performance in both simulations and experiments. Note that $\beta_{v,on}$ should be chosen significantly lower than 1 in order to allow for natural oscillations about the nominal propeller loading due to time-varying inflow to the propeller.

5.2 Anti-spin Thruster Control

The torque and power controllers, although advantageous for normal operating conditions, will show unacceptable behavior when subject to large thrust losses. The nature of this problem is in many ways similar to that of a car wheel losing traction on a slippery surface during acceleration or braking (Smogeli et al., 2008). The work on anti-spin thruster control has therefore been motivated by similar control strategies in car anti-spin and ABS braking systems, see for example Haskara et al. (2000). With any of the core controllers from Section 4 in use for normal operating conditions, the proposed anti-spin control scheme is divided in two:

1. Primary anti-spin action: override the core controller and take control of the shaft speed.
2. Secondary anti-spin action: lower the setpoint of the controller to reduce the shaft speed.

5.2.1 Primary Anti-spin Action

If a ventilation incident is detected by the detection algorithm in (30), the desired primary anti-spin control action is to take control of the shaft speed until the ventilation has terminated. This is done by modifying the core controller output Q_{ci} in (10) with a torque scaling factor γ:

$$Q_{cas} = \gamma Q_{ci}, \tag{31}$$

where Q_{cas} is the anti-spin commanded torque, and γ is proposed as:

$$\gamma = \begin{cases} 1 & \text{for} \quad \zeta = 0 \quad \text{(not ventilated)}, \\ \hat{\beta}_Q & \text{for} \quad \zeta = 1 \quad \text{(ventilated)}. \end{cases} \tag{32}$$

In Smogeli and Sørensen (2009) it is shown that the anti-spin control law will give a bounded shaft speed during ventilation.

5.2.2 Secondary Anti-spin Action: Setpoint Mapping

For optimization of thrust production and reduction of wear and tear due to dynamic propeller loading during ventilation, it may desirable to reduce the propeller shaft speed. This can be done by modifying the thrust reference during ventilation, since the primary anti-spin control action assures that the shaft speed is kept close to its reference. The desired shaft speed during ventilation, n_{as}, will be a thruster specific parameter, and must be chosen as a trade-off between thrust production, wear and tear, and response time. The nominal shaft speed reference n_r from (13) should not be changed to n_{as} instantaneously, as this will lead to undesired transients. It is therefore proposed to add a low-pass filter with time constant τ_n and a rate limiting algorithm to the change from n_r to n_{as} at ventilation detection, and from n_{as} to n_r at ventilation termination. The filtered and rate limited shaft speed reference is termed n_{ras}, i.e. $\dot{n}_{fall} < \dot{n}_{ras} < \dot{n}_{rise}$, where $\dot{n}_{fall}$ and $\dot{n}_{rise}$ are the rate limits. The thrust reference corresponding to n_{ras} is termed T_{ras}, and is given by (7a) with K_{T0} replaced by K_{TC}:

$$T_{ras} = \text{sign}(n_{ras}) K_{TC} \rho D^4 n_{ras}^2. \tag{33}$$

Since (33) is the inverse of (13), $T_{ras} \equiv T_r$ when ventilation is not detected.

5.2.3 Implementation Aspects

Perfect shaft speed control during ventilation would be possible if the ventilation incident could be foreseen, and $\beta_Q(t, \omega)$ was known. However, since the propeller torque is not available as a measurement, and the ventilation incidents are random processes caused by wave elevation and vessel motion, this is not possible. An implementable solution is to use the torque loss estimation and ventilation detection schemes. The deviation of the shaft speed from the steady-state solution will then depend on the deviation of the torque modification factor γ from the actual torque loss factor $\beta_Q(t, \omega)$ during ventilation.

To achieve the best possible control over the shaft speed during ventilation, γ should be switched from 1 to $\hat{\beta}_Q$ immediately when ventilation is detected. However, in order to avoid transients in the control input, the transition of γ from 1 to $\hat{\beta}_Q$ at ventilation detection, and from $\hat{\beta}_Q$ to 1 at ventilation termination, should be rate limited, i.e. $\dot{\gamma}_{fall} < \dot{\gamma} < \dot{\gamma}_{rise}$. The rate limits $\dot{\gamma}_{rise}$ and $\dot{\gamma}_{fall}$ would typically be of magnitude 1. Furthermore, to avoid using the potentially noisy estimate $\hat{\beta}_Q$ directly in the control law, it may be beneficial to filter γ by a properly chosen low-pass filter with time constant τ_γ.

A block diagram of the resulting thruster controller with anti-spin is shown in Figure 3. Note that the proposed anti-spin controller may be used with all the core controllers from Section 4.

Remark 2 *A well-tuned shaft speed controller will produce a controller output similar to the proposed anti-spin controller in (31) during ventilation, since the objective of the shaft speed controller is to keep the shaft speed constant, regardless of the load disturbance. However, since it is desired to use torque and power control in normal conditions, using a shaft speed controller during ventilation would require switching between the two controllers. This approach is further discussed in Smogeli (2006). If shaft speed control is chosen for normal conditions, anti-spin control may not be necessary.*

6 SENSITIVITY TO THRUST LOSSES

The steady-state performance of the controllers presented above can be theoretically analyzed by establishing the sensitivity to various thrust loss effects. Depending on the controller, a loss of propeller loading may, in addition to changes in propeller thrust and torque, lead to changes in shaft speed and power. As proposed by Sørensen et al. (1997) the relationship between the actual and reference

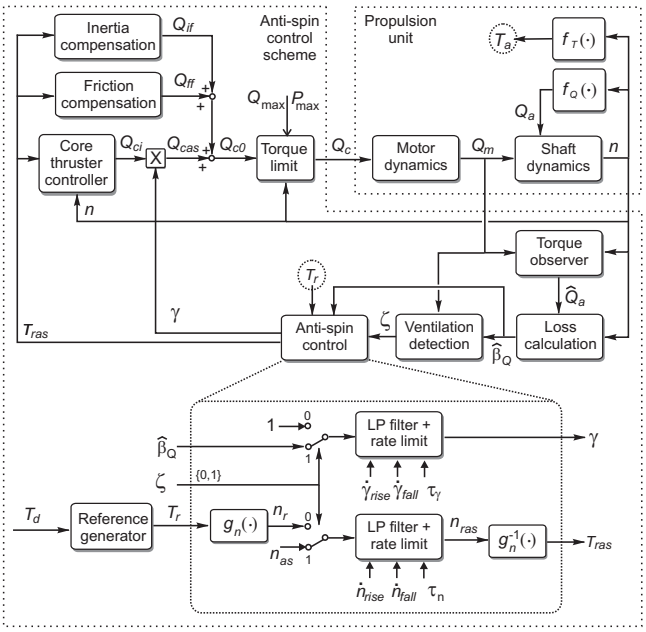

Figure 3: The anti-spin control scheme, including core controller, torque observer, loss calculation, ventilation detection, and anti-spin control actions.

thrust, torque, shaft speed, and power are termed sensitivity functions.

When developing the steady-state sensitivity functions (Smogeli, 2006) it is assumed that all controllers obtain their objectives perfectly, i.e. $n = n_r$ for shaft speed control, $Q_a = Q_r$ for torque control, and $P_a = P_r$ for power control. It has hence been assumed that the friction is perfectly compensated for in torque and power control, i.e. $Q_{ff} = Q_f$.

Assuming that all controllers perform ideally, the steady-state sensitivity functions for speed control, torque control and power control are shown in Table 1. For details in the derivation of the sensitivity functions, see Sørensen et al. (1997) and Smogeli (2006).

Remark 3 *It is interesting to note that if the controllers have knowledge of the instantaneous values of K_T and K_Q, such that $K_{TC} = K_T$ and $K_{QC} = K_Q$ at all times, all sensitivity functions reduce to unity, since n_r from (13), Q_r from (21), and P_r from (23) will be equal to the true values n, Q_a, and P_a. This means that all controllers perform identically. Also notice that $sn_i(\cdot)sq_i(\cdot) \equiv sp_i(\cdot)$ for all controllers, as should be expected.*

7 EXPERIMENTS

This section presents experimental results with the controllers designed above. The importance of the friction compensation scheme is investigated, and the dynamic performance of the controllers in various operating conditions tested.

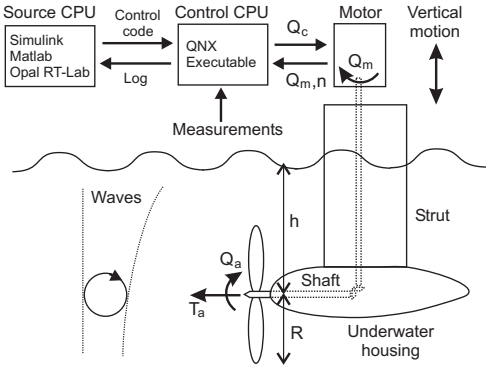

Figure 4: Sketch of the experimental setup.

D [m]	K_{T0}	K_{Q0}	I_s [kgm^2]	Q_s[Nm]	K_ω[Nms]
0.25	0.513	0.0444	0.05	1.0	0.01

Table 2: Main propeller data.

The majority of the experiments were conducted for shaft speed control, torque control, and power control, since the main purpose of this work was to test the properties of the basic thruster control methods. The combined torque/power controller was also tested, and behaved exactly as expected. Its performance can be inferred from the performance of the torque and power controllers.

7.1 Experimental Setup

The experiments were conducted in the Marine Cybernetics Laboratory (MCLab) at NTNU. The MCLab basin is 40m long, 6.45m wide, and 1.5m deep, and is equipped with a towing carriage and a wave-maker system. Two types of setups were used during the various tests. The tested propeller was of conventional design with 4 blades, pitch ratio at 70% of the propeller radius $P/D = 1.0$, and expanded blade area ratio $EAR = 0.55$. The propeller was tested both with and without duct. For the results presented here a duct was used for the anti-spin tests only. The propeller was attached to a shaft equipped with thrust and torque sensors inside an underwater housing, and driven by an electric motor via shafts and gears with gear ratio 1:1. The rig with motor, gears, underwater housing, shaft and propeller was fixed to the towing carriage on a vertical slide, which was used to control the submergence of the propeller relative to the free surface. Ventilation incidents could hence be generated by moving the propeller vertically with a calm free surface. The motor torque was controlled from a PC onboard the carriage, using feedback from the propeller shaft speed and the motor torque. The control code was generated by rapid prototyping using Opal RT-Lab and source code in Matlab/Simulink. A sketch of the experimental setup is given in Fig. 4.

The main characteristics of the ducted propeller and drive system are summarized in Table 2. The nominal thrust

Sensitivity	Speed control	Torque control	Power control
Thrust: $st_i(\cdot) \triangleq \frac{T_a}{T_r}$	$st_n(\cdot) = \frac{K_T}{K_{TC}}$	$st_q(\cdot) = \frac{K_T}{K_{TC}}\frac{K_{QC}}{K_Q}$	$st_p(\cdot) = \frac{K_T}{K_{TC}}(\frac{K_{QC}}{K_Q})^{2/3}$
Speed: $sn_i(\cdot) \triangleq \frac{n}{n_r}$	$sn_n(\cdot) = 1$	$sn_q(\cdot) = \sqrt{\frac{K_{QC}}{K_Q}}$	$sn_p(\cdot) = \frac{K_{QC}^{1/3}}{K_Q^{1/3}}$
Torque: $sq_i(\cdot) \triangleq \frac{Q_a}{Q_r}$	$sq_n(\cdot) = \frac{K_Q}{K_{QC}}$	$sq_q(\cdot) = 1$	$sq_p(\cdot) = \frac{K_Q^{1/3}}{K_{QC}^{1/3}}$
Power: $sp_i(\cdot) \triangleq \frac{P_a}{P_r}$	$sp_n(\cdot) = \frac{K_Q}{K_{QC}}$	$sp_q(\cdot) = \frac{K_{QC}^{1/2}}{K_Q^{1/2}}$	$sp_p(\cdot) = 1$

Table 1: Sensitivity functions, where i=n for shaft speed control, i=q for torque control, i=p for power control, and i=c for combined torque/power control

and torque coefficients for the propeller without duct were found to be $K_{T0} = 0.570$ and $K_{Q0} = 0.0750$. The nominal thrust and torque coefficients for reversed thrust were found to be $K_{T0r} = 0.393$ and $K_{Q0r} = 0.0655$.

7.1.1 Friction

In the experiments presented here, the shaft friction turned out to affect the performance of the torque and power controllers. A feedforward friction compensation scheme as proposed in Section 4.5 was therefore implemented. Over the course of the experiments, the friction compensation coefficients were found to be in the range $Q_{f0} \in [0.8, 1.0]$ and $Q_{f1} \in [0.009, 0.011]$.

7.1.2 Control Parameters

The control coefficients K_{TC} and K_{QC} used in the experiments were as given by (11), with the half "width" of the transition region $n_c = 3$. The rotational inertia of the model-scale propeller was not found to be a dominating term. Hence, the inertia compensation scheme in (15) was not needed. Therefore, and since only feasible thrust reference trajectories were used, no reference generator as in (14) was used. The constant plus linear friction compensation scheme (16) was used, with Q_{f0} and Q_{f1} appropriately chosen in the range specified above. The switching "width" of the smooth switching function in (17) was chosen as $n_s = 0.5$. The shaft speed PI controller parameters (20) were chosen as $K_p = 0.2$ and $T_i = 0.05$ s, which gave adequate tracking properties. For the combined controller (25), the weighting function parameters (26) were chosen as $[r, p, k] = [4, 0.5, 1]$. This gave a pure torque controller for $n < 0.5$ and a pure power controller for $n > 3$.

The friction compensation was chosen with $Q_{f0s} = 1.0$Nm and $Q_{f1} = 0.01$Nms. The inertia compensation was not needed for the small model-scale propeller. The control coefficients were chosen as $K_{TC} = K_{T0} = 0.513$ and $K_{QC} = K_{Q0} = 0.0444$. For the combined controller (25), the weighting function parameters (26) were chosen as $[r, p, k] = [4, 0.5, 1]$. This gave a pure torque controller for $n < 0.5$rps and a pure power controller for $n > 3$rps. The shaft speed PI controller parameters (20) were chosen as $K_p = 0.2$ and $T_i = 0.05$s.

In the load torque observer, the gains were chosen as $k_a = 15$ and $k_b = -25$. In the ventilation detection scheme, the parameters were chosen as $\beta_{v,on} = 0.6$ and $\beta_{v,off} = 0.9$, and the detection delay was set to $T_{vent} = 1$s. For the proposed anti-spin controller, the settings for the primary anti-spin action were $\dot{\gamma}_{rise} = 1\text{s}^{-1}$, $\dot{\gamma}_{fall} = -1\text{s}^{-1}$, and unless otherwise stated $\tau_\gamma = 0.3$s. For the secondary anti-spin action, the filter time constant was chosen as $\tau_n = 0.05$s, and the rate limits were chosen as $\dot{n}_{rise} = 3\text{s}^{-2}$ and $\dot{n}_{fall} = -3\text{s}^{-2}$. The desired shaft speed during ventilation was set to $n_{as} = 9$rps. The latter choice was motivated from observations during the tests, where it seemed that the most violent dynamic loading disappeared below 10rps. A maximum shaft speed of $n_{\max} = 25$rps was enforced.

The anti-spin control scheme appears to be robust to parameter tuning. In order to avoid detection chattering, however, it is important not to choose $\beta_{v,on}$ too large. In addition, if the rate limits are chosen too low or the filter time constants too large, the anti-spin controller response will become slow, and the shaft speed will be allowed to increase more during ventilation. A further discussion and guidelines on tuning are given in Smogeli (2006).

7.2 Quasi-static Tests

In these tests the thrust reference was kept constant at $T_r = 100$N, the advance velocities were $V_a = \{-1, -0.5, 0, 0.5, 1, 1.5\}$ m/s, and the speed, torque, and power controllers were used. Each combination was run 3 times, giving a total of 54 runs. The tests showed excellent repeatability. The length of the test series were limited by the length of the basin, but gave adequate statistical values.

The performance of the three controllers are summed up in Figure 5, where the propeller thrust T_a, propeller torque Q_a, shaft speed n, motor torque Q_m, and motor power P_m are shown for varying advance speeds. The friction compensation is not included in the plots of motor torque and power. It is clear that the three controllers obtain their objectives: the shaft speed controller keeps the shaft speed most constant, the torque controller keeps the motor torque most constant, and the power controller keeps the motor power most constant. As the advance speed increases, the effective angle of attack of the propeller blades is decreased, and the propeller loading decreases for a constant shaft speed. This can be seen in terms of reduced propeller thrust and torque at increasing advance velocities for the

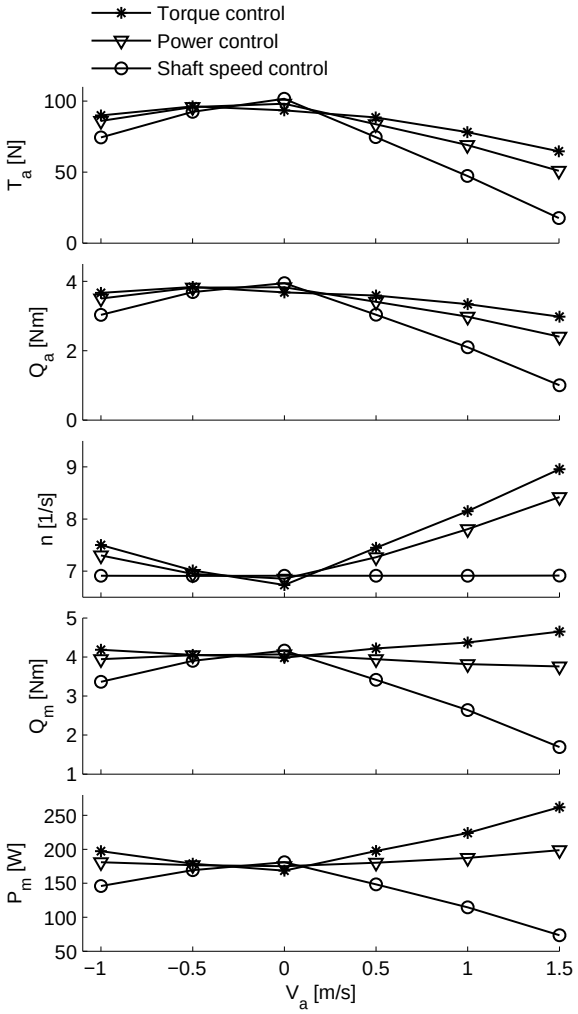

Figure 5: Comparison of propeller thrust T_a, torque Q_a, shaft speed n, motor torque Q_m and power P_m for the shaft speed, torque and power controllers in varying advance velocities V_a.

shaft speed controller: at $V_a = 1.5$ m/s, the propeller thrust is reduced from 100 N to 18 N. The torque and power controllers have much better performance, since the controllers increase the shaft speed as the propeller loading decreases: at $V_a = 1.5$ m/s, the propeller thrust is reduced from 100 N to 65 N and 50 N respectively.

7.3 Dynamic Tests in Waves

To validate the dynamic performance of the controllers when subject to rapidly changing inflow to the propeller a total of 34 tests in regular and irregular waves were performed. The thrust reference was $T_r = 90$ N and the carriage was kept stationary. A comparison of the controller performance in regular waves with wave height 8 cm and period 1 s is shown in Figure 6. The results are summarized in the following:

- The shaft speed controller keeps the shaft speed constant, and has to vary the motor torque and power in order to achieve this. The resulting propeller thrust and torque have the largest variance.

- The torque controller keeps the motor torque constant, and as a result the shaft speed varies with the loading. The resulting propeller thrust and torque have the smallest variance.

- The power controller keeps the motor power constant, and as a result both the shaft speed and motor torque varies with the loading. The resulting propeller thrust and torque lie between the shaft speed and torque controller values.

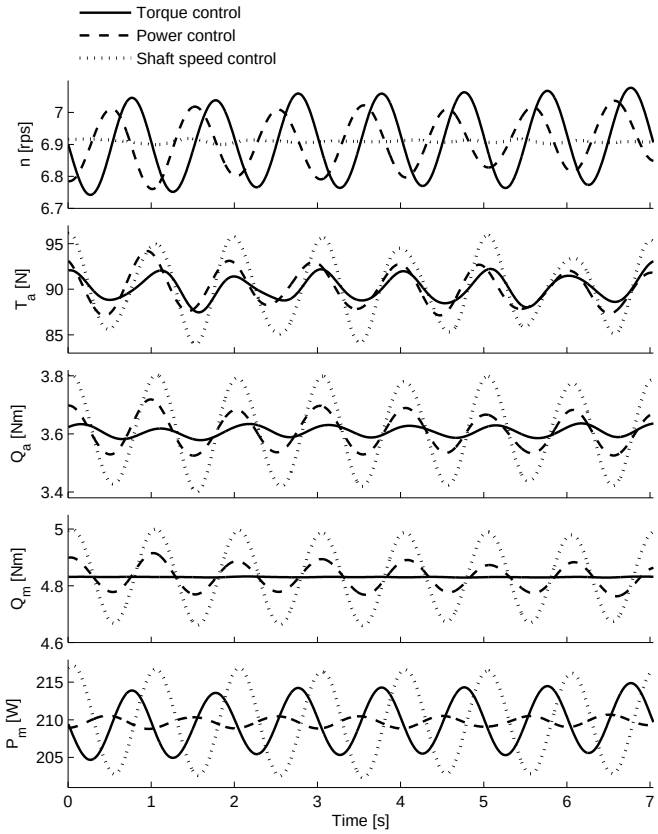

Figure 6: Comparison of shaft speed, torque, and power control in regular waves.

Tests with time-varying thrust reference trajectories are presented in Smogeli (2006) and Sørensen and Smogeli (2009).

7.4 Anti-spin Tests

The anti-spin control scheme was tested in a variety of operating conditions: for constant and time-varying thrust references, in waves, with a calm free surface and forced vertical motion of varying amplitude A_v, period T_v, and mean submergence h_0, and in combinations of waves and vertical motion. In the results presented here, the thrust reference was kept constant during forced vertical motion with

a calm free surface. This improved repeatability and enabled comparison of the various controllers, since the time series could be synchronized by comparing the relative vertical motion of the propeller. Because of the chaotic nature of ventilation, the actual operational conditions for the propeller vary from one test run to another. However, the repeatability is in general good. The results presented below are for $h_0 = 15$cm, $A_v = 15$cm, and $T_v = 5$s. Performance comparisons in other conditions, further validating the robust performance of the anti-spin controller, are presented in Smogeli (2006).

Figure 7 shows comparisons of the thrust T_a, propeller torque Q_a, shaft speed n, motor torque Q_m, and motor power P_m for four different thruster controllers during a ventilation incident with $T_r = 200$N. The ventilation incident starts at $t \approx 11.2$s, and terminates at $t \approx 14.5$s. The compared controllers are shaft speed PI control (20), torque control (21), power control (24), and the proposed anti-spin controller based on combined torque/power control (25). With anti-spin activated, both the primary (31) and the secondary (33) anti-spin actions were used. The time series show that the torque controller and the power controller both lead to propeller racing. The shaft speed controller and the anti-spin controller limit the shaft speed as intended, with the secondary anti-spin action giving a slightly reduced shaft speed during ventilation. The resulting thrust during ventilation is about the same for all controllers. That is, the anti-spin controller, which reduces the shaft speed to 9rps during ventilation, produces the same thrust as the torque controller, which races to the imposed limit of 25rps. This corresponds well to the experimental results shown in Fig. 1. The power consumption of the torque controller is unacceptably high, whereas the power controller keeps the power consumption limited. The shaft speed and anti-spin controllers give a lower power consumption during ventilation, but this is not considered to be a problem.

Figure 8 shows comparisons of T_a, Q_a, n, Q_m, and P_m for four controllers during a ventilation incident with $T_r = 300$N: power control, combined control with primary anti-spin action only (marked P), combined control with primary and secondary anti-spin action (marked P+S), and shaft speed control. The torque controller could not be tested for this thrust reference, since the propeller racing was too severe to give sensible results. The ventilation incident starts at $t \approx 16.2$s, and terminates at $t \approx 19.5$s. Again, the thrust levels during ventilation are almost identical for all the controllers. It can be noted that the primary anti-spin controller and the shaft speed controller behave almost identically, confirming that the proposed anti-spin controller has a similar performance as a well-tuned shaft speed PI controller during ventilation. The secondary anti-spin action lowers the shaft speed as intended during ventilation. Figure 9 shows details from the anti-spin controller

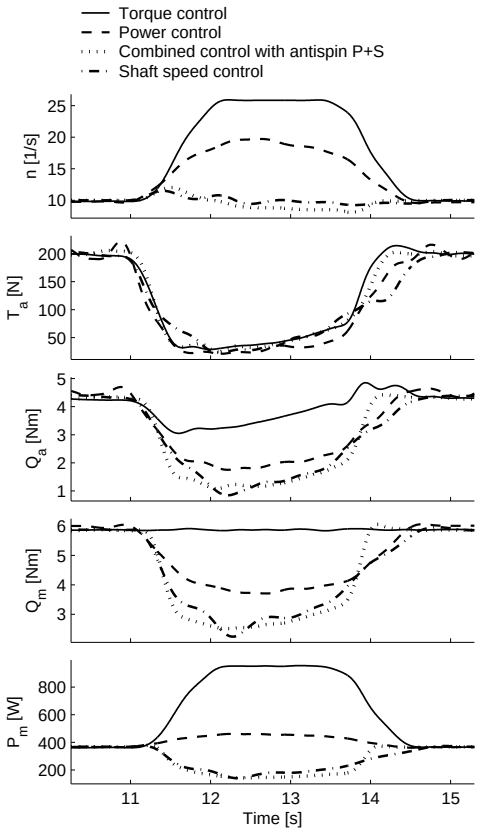

Figure 7: Comparison of four controllers during a ventilation incident at $T_r = 200$N.

during a ventilation incident: propeller torque Q_a versus estimated propeller torque $\hat{Q}_a$, estimated torque loss factor $\hat{\beta}_Q$ and ventilation detection signal ζ, torque modification factor γ, deviation of γ from the measured β_Q, and the desired shaft speed n_{ras}. The time series show that the anti-spin controller, including torque observer and ventilation detection, performs as intended.

8 CONCLUSIONS

Low-level controllers based on shaft speed, torque, and power control for electrically driven thrusters on vessels in normal operating conditions have been investigated, and evaluated according to three main performance criteria. The conventional shaft speed controller gave the thrust, torque, and power with the largest variance, and it was the least robust to disturbances in the in-line flow velocity. The torque controller produced the thrust and torque with the smallest variance, and was superior with respect to compensating for thrust losses due to disturbances in the inflow. The power controller gave the least oscillations in the power, with the resulting propeller thrust and torque in-between the shaft speed and torque controller values. The combined torque and power controller gave the overall best improvement in the performance from low to high loadings. Steady-state sensitivity functions describing the

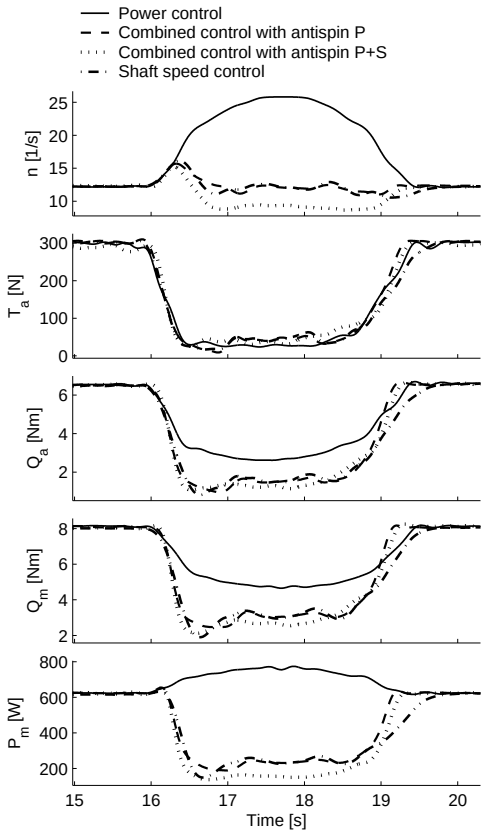

Figure 8: Comparison of four controllers during a ventilation incident at $T_r = 300$N.

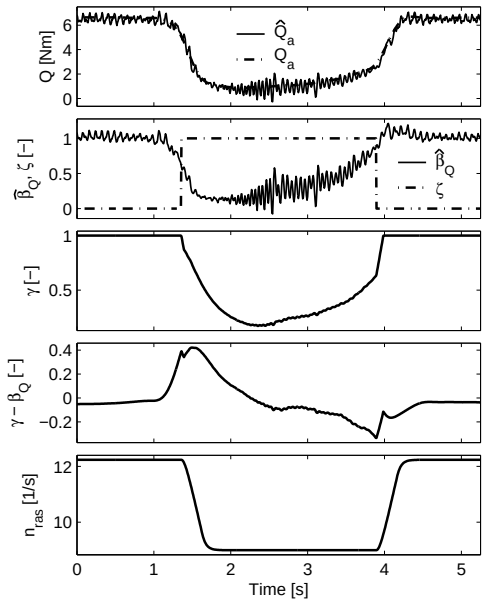

Figure 9: Time series of the main parameters in the anti-spin control law with primary and secondary control action during a ventilation incident at $T_r = 300$N.

performance of the various controllers in terms of resulting thrust, shaft speed, torque, and power when subject to thrust losses were presented. Experiments illustrated the difference in performance and robustness of the different controllers.

It has been shown that torque and power control is a feasible solution for high-performance thruster control only if special precautions are taken during extreme environmental conditions, when the propeller may be subject to ventilation and in-and-out-of water effects. To solve this problem, an anti-spin thruster controller has been designed. The thruster performance was monitored by a load torque observer, and the anti-spin controller was triggered by a ventilation detection scheme. The anti-spin controller took control of and lowered the shaft speed. Experiments with a model scale propeller were presented. The results showed that the torque and power controllers with anti-spin had comparable performance to that of a well-tuned shaft speed PI controller during ventilation, without compromising the superior performance of torque and power control in normal conditions.

9 ACKNOWLEDGMENT

This work has been carried out at the Centre for Ships and Ocean Structures (CeSOS) at NTNU in cooperation with the research project Energy-Efficient All-Electric Ship (EEAES). The Research Council of Norway is acknowledged as the main sponsor of CeSOS and EEAES.

REFERENCES

Bachmayer, R., Whitcomb, L. L., and Grosenbaugh, M. A. (2000). An Accurate Four-Quadrant Nonlinear Dynamical Model for Marine Thrusters: Theory and Experimental Validation. IEEE Journal of Oceanic Engineering, 25(1):146–159.

Bakkeheim, J., Johansen, T. A., Smogeli, O. N., and Sørensen, A. J. (2008). Lyapunov-based Integrator Resetting with Application to Marine Thruster Control. IEEE Trans. Control Systems Technology. Accepted for publication.

Blanke, M. (1994). Optimal Speed Control for Cruising. In Proc. 3^{rd} IFAC Conference on Manoeuvring and Control of Marine Craft (MCMC'94), pages 125–134, Southampton, UK.

Blanke, M. and Busk Nielsen, P. (1987). Electronic Governor Control for two stroke Engines. In Nordisk Sjöfartsteknisk Årsbok – Svensk Sjöfarts Tidning, volume 40, pages 82–84.

Blanke, M. and Busk Nielsen, P. (1990). The Marine Engine Governor. In Proc. 2nd Int. Conf. on Maritime Communications and Control, pages 11–20, London, UK.

Blanke, M., Pivano, L., and Johansen, T. (2007). An Efficiency Optimizing Propeller Speed Control for Ships in Moderate Seas - Model Experiments and Simulation. In Proc. IFAC Conference on Control Applications in Marine Systems (CAMS'07), Bol Croatia.

Brix, J. (1978). Querstrahlsteuer. Forschungzentrum des Deutschen Schiffbaus, Bericht Nr. 80. In German. "Steering with Lateral Thrusters".

Chislett, M. S. and Björheden, O. (1966). Influence of Ship Speed on the Effectiveness of a Lateral-Thrust Unit. Hydro- og Aerodynamisk Laboratorium Report No Hy-8, Lyngby, Denmark.

Faltinsen, O. M., Minsaas, K. J., Liapis, N., and Skjørdal, S. O. (1980). Prediction of resistance and propulsion of a ship in a seaway. In Proceedings of the Thirteenth Symposium on Naval Hydrodynamics, Tokyo.

Fossen, T. I. and Blanke, M. (2000). Nonlinear Output Feedback Control of Underwater Vehicle Propellers Using Feedback From Estimated Axial Flow Velocity. IEEE Journal of Oceanic Engineering, 25(2):241–255.

Haskara, I., Özgüner, U., and Winkelman, J. (2000). Wheel Slip Control for Antispin Acceleration via Dynamic Spark Advance. Control Engineering Practice, 8:1135–1148.

Healey, A. J., Rock, S. M., Cody., S., Miles, D., and Brown, J. P. (1995). Toward an improved understanding of thruster dynamics for underwater vehicles. IEEE Journal of Oceanic Engineering, 29(4):354–361.

Hespanha, J. P. and Morse, A. S. (2002). Switching between stabilizing controllers. Automatica, 38(11):1905–1917.

Koushan, K. (2004). Environmental and Interaction Effects on Propulsion Systems used in Dynamic Positioning, an Overview. In Proc. 9^{th} Int. Symp. Practical Design of Ships and Other Floating Structures (PRADS'04), pages 1013–1020, Lübeck-Travemünde, Germany.

Lehn, E. (1992). FPS-2000 Mooring and Positioning, Part 1.6 Dynamic Positioning - Thruster Efficiency: Practical Methods for Estimation of Thrust Losses. Technical Report 513003.00.06, Marintek, SINTEF, Trondheim, Norway.

Leonhard, W. (1996). Control of Electrical Drives. Springer-Verlag, Berlin, 2^{nd} edition.

Minsaas, K. J., Thon, H. J., and Kauczynski, W. (1987). Estimation of Required Thruster Capacity for Operation of Offshore Vessels under Severe Weather Conditions. In Proc. 3^{rd} Int. Symp. Practical Design of Ship and Mobile Units (PRADS'87), pages 411–427, Trondheim, Norway.

Olofsson, N. (1996). Force and Flow Characteristics of a Partially Submerged Propeller. PhD thesis, Chalmers University of Technology, Göteborg, Sweden.

Pivano, L. (2008). Thrust Estimation and Control of Marine Propellers in Four-Quadrant Operations. PhD thesis, Department of Engineering Cybernetics, Norwegian University of Science and Technology (NTNU), Thesis 2008:20, Trondheim, Norway.

Ruth, E. (2008). Propulsion Control and Thrust Allocation on Marine Vessels. PhD thesis, Department of Marine Technology, Norwegian University of Science and Technology (NTNU), Thesis 2008:203, Trondheim, Norway.

Ruth, E. and Smogeli, Ø. N. (2006). Ventilation of Controllable Pitch Thrusters. SNAME Marine Technology, 43(4):170–179.

Ruth, E., Smogeli, Ø. N., and Sørensen, A. J. (2006). Overview of Propulsion Control for Surface Vessels. In Proc. 7^{th} IFAC Conference on Manoeuvring and Control of Marine Craft (MCMC'06), Lisbon, Portugal.

Shiba, H. (1953). Air-Drawing of Marine Propellers. In Report of Transportation Technical Research Institute, The Unyu-Gijutsu Kenkyujo, Japan.

Smogeli, Ø. N. (2006). Control of Marine Propellers: from Normal to Extreme Conditions. PhD thesis, Department of Marine Technology, Norwegian University of Science and Technology (NTNU), Thesis 2006:187, Trondheim, Norway.

Smogeli, Ø. N., Aarseth, L., Overå, E. S., Sørensen, A. J., and Minsaas, K. J. (2003). Anti-spin Thruster Control in Extreme Seas. In Proc. 6^{th} IFAC Conference on Manoeuvring and Control of Marine Craft (MCMC'03), pages 221–226, Girona, Spain.

Smogeli, Ø. N., Hansen, J., Sørensen, A. J., and Johansen, T. A. (2004a). Anti-Spin Control for Marine Propulsion Systems. In Proc. 43^{rd} IEEE Conference on Decision and Control (CDC'04), Paradise Island, Bahamas.

Smogeli, Ø. N., Ruth, E., and Sørensen, A. J. (2005). Experimental Validation of Power and Torque Thruster Control. In Proc. Mediterranean Conference on Control and Automation (MED'05), Limassol, Cyprus.

Smogeli, Ø. N. and Sørensen, A. J. (2009). Anti-Spin Thruster Control for Ships. IEEE Transactions on Control Systems Technology. Accepted for publication.

Smogeli, Ø. N., Sørensen, A. J., and Fossen, T. I. (2004b). Design of a Hybrid Power/Torque Thruster Controller with Thrust Loss Estimation. In Proc. IFAC Conference on Control Applications in Marine Systems (CAMS'04), Ancona, Italy.

Smogeli, Ø. N., Sørensen, A. J., and Minsaas, K. J. (2008). The Concept of Anti-Spin Thruster Control. Control Engineering Practice, 16(4):465–481.

Sørensen, A. J. (2005). Structural Issues in the Design and Operation of Marine Control Systems. IFAC Journal of Annual Reviews in Control, 29(1):125–149.

Sørensen, A. J., Ådnanes, A. K., Fossen, T. I., and Strand, J. P. (1997). A New Method of Thruster Control in Positioning of Ships based on Power Control. In Proc. 4^{th} IFAC Conference on Manoeuvring and Control of Marine Craft (MCMC'97), Brijuni, Croatia.

Sørensen, A. J. and Smogeli, Ø. N. (2009). Torque and Power Control of Electrically Driven Marine Propellers with Experimental Validation. Control Engineering Practice. Accepted for publication.

Whitcomb, L. L. and Yoerger, D. R. (1999a). Development, Comparison, and Preliminary Experimental Validation of Nonlinear Dynamic Thruster Models. IEEE Journal of Oceanic Engineering, 24(4):481–494.

Whitcomb, L. L. and Yoerger, D. R. (1999b). Preliminary Experiments in Model-Based Thruster Control for Underwater Vehicle Positioning. IEEE Journal of Oceanic Engineering, 24(4):495–506.

Yoerger, D. R., Cooke, J. G., and Slotine, J. J. E. (1991). The Influence of Thruster Dynamics on Underwater Vehicle Behavior and Their Incorporation Into Control System Design. IEEE Journal of Oceanic Engineering, 15(3):167–179.